Earth and Planetary Science Letters 474 (2017) 128–137

Contents lists available at ScienceDirect

Earth and Planetary Science Letters

www.elsevier.com/locate/epsl

Calcium isotopic fractionation in mantle peridotites by melting and metasomatism and Ca isotope composition of the Bulk Silicate Earth

Jin-Ting Kang [a,b], Dmitri A. Ionov [c], Fang Liu [b,d], Chen-Lei Zhang [b,d], Alexander V. Golovin [e,f,g], Li-Ping Qin [a], Zhao-Feng Zhang [b,*], Fang Huang [a,*]

[a] CAS Key Laboratory of Crust-Mantle Materials and Environments, School of Earth and Space Sciences, University of Science and Technology of China, Hefei 230026, China
[b] State Key Laboratory of Isotope Geochemistry, Guangzhou Institute of Geochemistry, the Chinese Academy of Sciences, Guangzhou 510640, China
[c] Géosciences Montpellier, Université de Montpellier, Montpellier 34095, France
[d] University of Chinese Academy of Sciences, Beijing 100049, China
[e] Sobolev Institute of Geology and Mineralogy, Siberian Branch Russian Academy of Sciences, Koptyuga 3, Novosibirsk 630090, Russian Federation
[f] Novosibirsk State University, Pirogova 2, Novosibirsk 630090, Russian Federation
[g] Diamond and Precious Metal Geology Institute, Siberian Branch Russian Academy of Sciences, Yakutsk 677007, Russian Federation

ARTICLE INFO

Article history:
Received 23 February 2017
Received in revised form 23 May 2017
Accepted 23 May 2017
Available online xxxx
Editor: F. Moynier

Keywords:
Ca isotopes
Bulk Silicate Earth
partial melting
metasomatism
lithospheric mantle
peridotite xenolith

ABSTRACT

To better constrain the Ca isotopic composition of the Bulk Silicate Earth (BSE) and explore the Ca isotope fractionation in the mantle, we determined the Ca isotopic composition of 28 peridotite xenoliths from Mongolia, southern Siberia and the Siberian craton. The samples are divided in three chemical groups: (1) fertile, unmetasomatized lherzolites (3.7–4.7 wt.% Al_2O_3); (2) moderately melt-depleted peridotites (1.3–3.0 wt.% Al_2O_3) with no or very limited metasomatism (LREE-depleted cpx); (3) strongly metasomatized peridotites (LREE-enriched cpx and bulk rock) further divided in subgroups 3a (harzburgites, 0.1–1.0% Al_2O_3) and 3b (fertile lherzolites, 3.9–4.3% Al_2O_3). In Group 1, $\delta^{44/40}$Ca of fertile spinel and garnet peridotites, which experienced little or no melting and metasomatism, show a limited variation from 0.90 to 0.99‰ (relative to SRM 915a) and an average of 0.94 ± 0.05‰ (2SD, $n = 14$), which defines the Ca isotopic composition of the BSE. In Group 2, the $\delta^{44/40}$Ca is the highest for three rocks with the lowest Al_2O_3, i.e. the greatest melt extraction degrees (average 1.06 ± 0.04‰, i.e. ~0.1‰ heavier than the BSE estimate). Simple modeling of modal melting shows that partial melting of the BSE with $10^3 \ln\alpha_{\text{peridotite-melt}}$ ranging from 0.10 to 0.25 can explain the Group 2 data. By contrast, $\delta^{44/40}$Ca in eight out of nine metasomatized Group 3 peridotites are lower than the BSE estimate. The Group 3a harzburgites show the greatest $\delta^{44/40}$Ca variation range (0.25–0.96‰), with $\delta^{44/40}$Ca positively correlated with CaO and negatively correlated with Ce/Eu. Chemical evidence suggests that the residual, melt-depleted, low-Ca protoliths of the Group 3a harzburgites were metasomatized, likely by carbonate-rich melts/fluids. We argue that such fluids may have low (≤0.25‰) $\delta^{44/40}$Ca either because they contain recycled crustal components or because Ca isotopes, similar to trace elements and their ratios, may be fractionated by kinetic and/or chromatographic effects of melt percolation in the mantle. The $\delta^{44/40}$Ca in Group 3b lherzolites (0.83–0.89‰) are lower than in the BSE as well, but the effects of metasomatism on $\delta^{44/40}$Ca are smaller, possibly because of the high Ca contents in their protoliths and/or smaller $\delta^{44/40}$Ca differences between the protoliths and metasomatic agents. The BSE estimates based on fertile peridotites in this study fall in the $\delta^{44/40}$Ca ranges for oceanic and continental basalts, various meteorites (achondrites; carbonaceous, ordinary and enstatite chondrites), Mars, and the Moon. These results provide benchmarks for the application of Ca isotopes to planet formation, mantle evolution, and crustal recycling.

1. Introduction

Calcium is an alkaline earth element with six stable isotopes: ^{40}Ca (96.941%), ^{42}Ca (0.657%), ^{43}Ca (0.135%), ^{44}Ca (2.086%), ^{46}Ca (0.004%) and ^{48}Ca (0.187%). Due to its high abundance in the

* Correspondence and requests for materials should be addressed to Fang Huang or Zhao-Feng Zhang.
E-mail addresses: zfzhang@gig.ac.cn (Z.-F. Zhang), fhuang@ustc.edu.cn (F. Huang).

http://dx.doi.org/10.1016/j.epsl.2017.05.035
0012-821X/

Earth (e.g. McDonough and Sun, 1995; Rudnick and Gao, 2003) and large relative mass-differences (~20% between ^{48}Ca and ^{40}Ca), Ca isotopes can be applied to studies of a number of fundamental geochemical processes. Because Ca is highly refractory with 50% condensation temperature (T_C) of 1517 K (Lodders, 2003), Ca isotope data on meteorites can be used to gain insights into planetary building blocks and the heterogeneity of the proto-planetary disk (e.g. Huang et al., 2012; Schiller et al., 2016; Simon and DePaolo, 2010; Valdes et al., 2014). Furthermore, because Ca isotopes can be strongly fractionated during low-temperature biological and surficial/supergene geological processes (e.g. Fantle and Tipper, 2014), they have the potential to trace recycled crustal materials in the deep Earth (e.g. DePaolo, 2004; Huang et al., 2011).

The mantle is the Earth's largest reservoir for Ca. Its Ca isotopic composition can be roughly assessed using oceanic basalts as 'probes' assuming that they represent the average isotopic signature of their mantle source regions, as was previously done for other metal stable isotope systems (e.g. Zn in Chen et al., 2013; Mg in Teng et al., 2007). The $\delta^{44/40}$Ca values [$\delta^{44/40}$Ca (‰) = $(^{44}Ca/^{40}Ca)_{sample}/(^{44}Ca/^{40}Ca)_{NIST\ SRM\ 915a} - 1$] reported for oceanic basalts range from 0.62 to 1.54‰ with an average of 0.90 ± 0.28‰ (2SD, $n = 61$) (Fig. 1; Amini et al., 2009; DePaolo, 2004; Holmden and Bélanger, 2010; Hindshaw et al., 2013; Huang et al., 2010, 2011; Jacobson et al., 2015; Skulan et al., 1997; Simon and DePaolo, 2010; Valdes et al., 2014). The large $\delta^{44/40}$Ca range for the basalts may indicate either broad Ca isotope variations in the mantle or, alternatively, that the basalts do not mirror the $\delta^{44/40}$Ca of their mantle sources due to isotope fractionation during partial melting and magma differentiation and/or addition of external components during magma emplacement. The average $\delta^{44/40}$Ca for the basalts is about 0.1‰ lower than the "upper mantle" value estimated by Huang et al. (2010) based on analyses of clinopyroxene (cpx) from two mantle xenoliths. However, due to the scarcity of data on $\delta^{44/40}$Ca in peridotites and the broad $\delta^{44/40}$Ca variations in the oceanic basalts, it is not clear yet if there is an isotopic offset between the basalts and the mantle. Even less certain may be attempts to infer the composition of the Bulk Silicate Earth (BSE) from data on oceanic basalts because their parental magmas are generated not from pristine but from depleted mantle possibly containing enriched components (e.g. Hofmann, 2014).

Recent studies of pyroxenes in mantle xenoliths from the US and China found considerable inter-mineral Ca isotopic fractionation, e.g. a broad range (0 to 1.1‰) of $\delta^{44/40}$Ca between cpx and orthopyroxene (opx) (Huang et al., 2010; Kang et al., 2016). Whole-rock $\delta^{44/40}$Ca estimated for the peridotites from the pyroxene data range from 0.7 to 1.1‰, but no whole-rock Ca isotope analyses of mantle xenoliths have been published as yet. $\delta^{44/40}$Ca for three peridotite reference materials (PCC-1, BM90/21-G and DTS-1) were reported by several studies and show ~0.5‰ variation (1.01–1.49‰) (e.g. Amini et al., 2009; Feng et al., 2017; He et al., 2017), yet it is not clear to what extent Ca isotopes in these materials were affected by late-stage processes like crustal contamination or low-temperature alteration. In addition, no Ca isotope data have been reported so far for garnet-facies peridotites, which are common at depths >60 km in the lithospheric mantle. Therefore, a sufficient number of appropriate peridotites need to be analyzed to precisely characterize the Ca isotopic composition of the upper mantle and the BSE.

Here, we report Ca isotope data on 28 well-characterized mantle peridotites from spinel and garnet depth facies and from cratonic and off-craton mantle. These samples represent major mantle rock types including (1) fertile spinel and garnet lherzolites, (2) melt-depleted, unmetasomatized lherzolites and harzburgites, and (3) strongly metasomatized refractory and fertile peridotites. We seek to constrain: (a) the Ca isotope composition of the BSE; (b) the range of Ca isotope variation in the continental lithospheric mantle; (c) the mechanisms responsible for the Ca isotope variations.

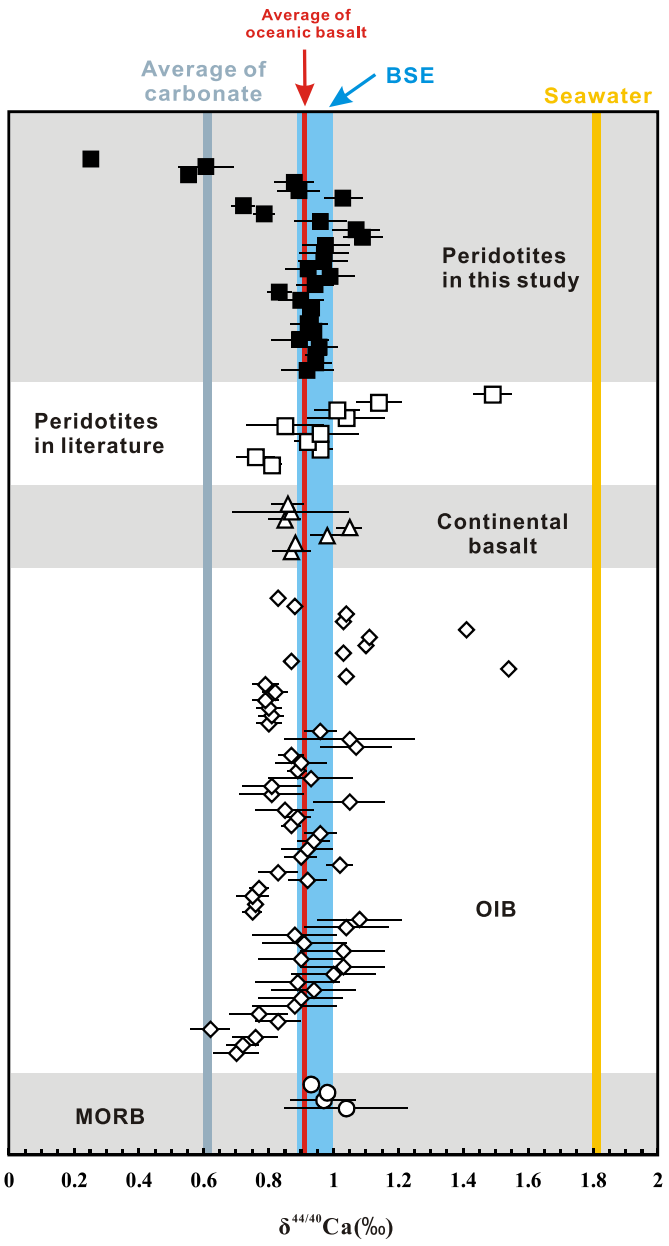

Fig. 1. A compilation of available Ca isotopic data for terrestrial basalts and peridotites. The red dashed line is the average of oceanic basalt of 0.90‰. The blue vertical band represents the $\delta^{44/40}$Ca of BSE estimated in this study. Data for basalts are from Skulan et al. (1997), Amini et al. (2009), Huang et al. (2010, 2011), Holmden and Bélanger (2010), Simon and DePaolo (2010), Hindshaw et al. (2013), Valdes et al. (2014) and Jacobson et al. (2015). Data for peridotites are from Amini et al. (2009) and Kang et al. (2016). The error bars are 2SE. The grey (left) and yellow (right) lines represent the average $\delta^{44/40}$Ca of marine carbonates and seawater. Note that marine carbonates have a broad range of $\delta^{44/40}$Ca from −1.09 to 1.81‰ (Fantle and Tipper, 2014 and references therein). For color codes refer to the online version of the paper.

Our results show that fertile peridotites have a consistent $\delta^{44/40}$Ca of 0.94 ± 0.05‰ (2SD, $n = 14$), which we propose as the BSE value. We further find that melt extraction at high melting degrees (>25%) may slightly elevate the $\delta^{44/40}$Ca values of peridotites while metasomatism may decrease their $\delta^{44/40}$Ca values, particularly in low-Ca rocks.

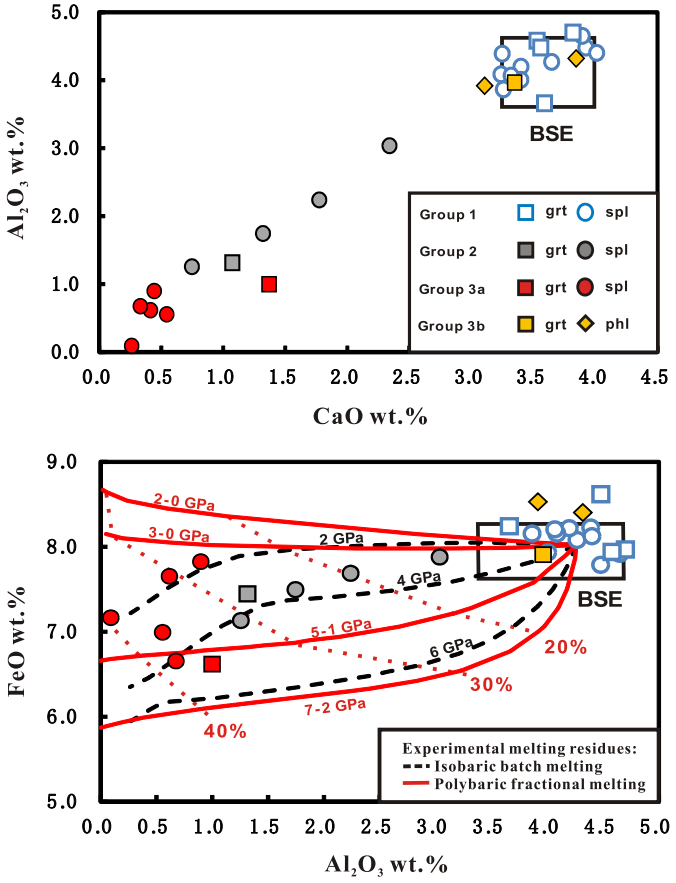

Fig. 2. Major element relations of whole-rock peridotites. Black dashed lines: isobaric batch melting residues at 2, 4 and 6 GPa (Herzberg, 2004); continuous red lines: residues of polybaric fractional melting at 2–0, 3–0, 5–1, and 7–2 GPa (Herzberg, 2004); red dotted lines: 20%, 30% and 40% melting degrees. See text for references for the BSE composition. The major element data of peridotites are from the literature (listed in Table 2) and unpublished data of DA Ionov and RW Carlson (for Tariat xenoliths). For color codes refer to the online version of the paper.

2. Geological background and sample description

The samples were selected from well-studied collections of mantle xenoliths from central and northeast Asia (see KML map) to represent the range of modal and chemical compositions of peridotite in the continental lithospheric mantle (CLM). The xenoliths are large, modally homogeneous, and show no or negligible alteration and/or contamination by host magma based on petrographic and chemical data. Locality, rock type, bulk-rock contents of Al_2O_3 and CaO, and data sources for each sample are given in Table 2; their CaO, Al_2O_3 and FeO contents are plotted in Fig. 2.

The majority of the xenoliths (23 out of 28) are from alkali basaltic pyroclastic rocks in three volcanic fields in central Asia: (1) Vitim east of Lake Baikal in Russia, (2) Tariat in central Mongolia and (3) Dariganga in southeast Mongolia. Three out of four Vitim xenoliths are fertile (3.7–4.6 wt.% Al_2O_3; 3.5–3.6 wt.% CaO) coarse garnet lherzolites hosted by 16 Ma old tuffs; sample 621-16 is a cpx-bearing garnet-spinel harzburgite (1.3 wt.% Al_2O_3, 1.07 wt.% CaO; ~3% cpx) from the 0.8 Ma old Yaksha volcano (Ionov, 2004; Ionov et al., 1993, 2005). Seventeen out of 18 Tariat xenoliths are from the 0.5 Ma old Shavaryn–Tsaram eruption center (labeled S, ST and STZ), one (H-25) is from the Holocene Haer volcano (Ionov, 2007). The Shavaryn–Tsaram site is famous for the abundance of large, fertile lherzolites brought up from a broad depth range (45–75 km) between the crust–mantle boundary and the garnet–spinel peridotite facies (Ionov et al., 1998; Press et al., 1986). Out of the 18 Tariat samples in this study, ten are fertile, cpx-rich spinel lherzolites, one (ST53389) is fertile garnet–spinel lherzolite, five range from low-cpx spinel lherzolites to harzburgites, and two more (4230-16 and 4230-19) are modally metasomatized fertile spinel lherzolites that contain ~2% of disseminated, texturally equilibrated phlogopite (phl) (Ionov et al., 1997). The single Dariganga xenolith (BN-8) in this study is a spinel harzburgite from the Barun-Nart eruption center (Ionov et al., 1992; Wiechert et al., 1997).

The other five samples are from the Udachnaya-East kimberlite in the central Siberian craton, Russia including a coarse garnet harzburgite (419/09), a cpx-bearing (107/03) and two apparently cpx-free (105/03, 137/08) spinel harzburgites, and a sheared garnet lherzolite (U85) (Doucet et al., 2012, 2013; Ionov et al., 2010).

In addition to the usual petrographic classification based on mineral assemblages and modal proportions, we identify 3 chemical groups among our samples based on their major oxide contents as well as rare earth element (REE) patterns (Table 2). REE patterns of peridotites are sensitive indicators of either melt extraction (depletion in light REE, LREE) because mineral/melt partition coefficients (K_d) for the highly incompatible LREE are an order of magnitude lower than for the moderately incompatible heavy REE (HREE) (see Ionov et al., 2002a, 2002b for references), or of metasomatism (LREE-enrichment) because metasomatic media are LREE-enriched. This is also the reason why some LREE may reside not in cpx, the main REE mineral host in spinel peridotites, but also in interstitial micro-phases (e.g. Hiraga et al., 2004), such that a bulk rock may have higher LREE/HREE than its cpx. Importantly, the behavior of Ca in the mantle is similar to that for the HREE, but distinct from the behavior of the LREE. In particular, if a rock is LREE-enriched, it does not necessarily imply that the metasomatism also affected its Ca budget. The share of Ca hosted by each mineral in our samples calculated from CaO measured in WR and in the minerals, and modal abundances are given in S-Table 1 of the Supplementary Material. These estimates show in particular that metasomatism may affect more the Ca budget of initially strongly melt-depleted, low-Ca harzburgites (e.g. by depositing interstitial materials) than that of high-Ca, cpx-rich lherzolites.

Group 1 rocks are fertile (3.7–4.7 wt.% Al_2O_3, 3.2–4.0 wt.% CaO), cpx-rich (14–20%) unmetasomatized lherzolites from Vitim and Tariat, including four garnet-bearing (9–13%), which have nearly flat whole-rock (WR) REE patterns and cpx depleted in LREE (Fig. 3a). These 14 samples are viewed as pristine (unmelted) mantle rocks or residues of low-degree partial melting. Over 90% of Ca in these rocks is hosted by the cpx (and garnet if present), 3–8% by opx and <2% by olivine.

Group 2 consists of five moderately melt-depleted (1.3–3.0 wt.% Al_2O_3, 0.75–2.3 wt.% CaO) lherzolites and harzburgites from Tariat, Vitim and Dariganga with slightly to moderately LREE-enriched WR patterns (but very low LREE well below those in primitive mantle) and LREE-depleted cpx patterns (Fig. 3b). The LREE depletion in the cpx indicates that this main carrier phase of Ca in the peridotites has not been significantly affected by metasomatism while the bulk-rocks may have been affected by ingress of LREE-bearing fluids, shortly before or during transport in host magma, along grain boundaries (e.g. Wiechert et al., 1997).

Group 3 includes two sub-groups of strongly metasomatized peridotites. Group 3a has six 'anhydrous' harzburgites from Tariat and Udachnaya, typically very low in Ca, with LREE-enriched WR as well as LREE-enriched and strongly fractionated cpx REE patterns (Fig. 3c). No cpx has been identified in thin sections in two of these samples, but it is possible that fine-grained cpx (or other Ca-rich phases) may be present in interstitial materials; only 14–24% of WR Ca is hosted by opx and olivine.

Group 3b combines two phl-spinel lherzolites from Tariat and a sheared garnet lherzolite from Udachnaya; all of them are 'fertile' in terms of major oxide contents (3.9–4.3 wt.% Al_2O_3; 3.1–3.9 wt.%

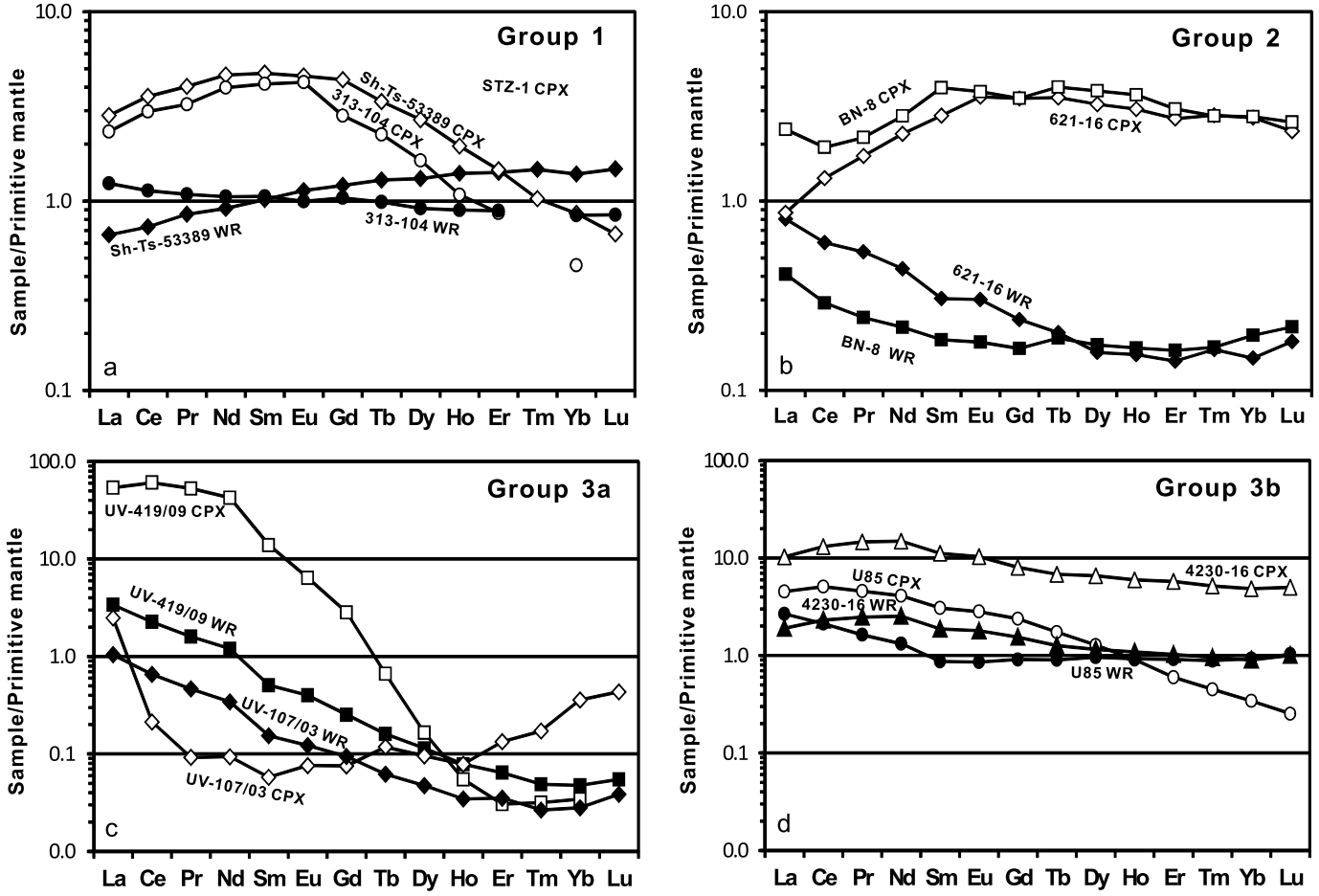

Fig. 3. Primitive mantle-normalized (McDonough and Sun, 1995) REE patterns of typical samples in Groups 1, 2, 3a and 3b: open symbols, clinopyroxene (cpx), filled symbols, whole-rocks.

CaO), but unlike Group 1 xenoliths, they have LREE-enriched WR and cpx patterns (Fig. 3d) with typical $(La/Nd)_N \geq 1$ or $(La/Ce)_N \geq 1$ in the cpx [the subscript N indicates normalization to primitive mantle (McDonough and Sun, 1995)] due to equilibration with LREE-rich silicate melts (Ionov and Hofmann, 1995; Ionov et al., 2002a, 2002b). Phl is very low in Ca, with cpx (plus garnet in U85) hosting ≥95% of Ca.

3. Analytical methods

Chemical purification and mass spectrometric analyses of Ca were done at the State Key Laboratory of Isotope Geochemistry, Guangzhou Institute of Geochemistry (GIG), Chinese Academy of Sciences (CAS). Ca isotope analyses were done on a thermal ionization mass-spectrometer (Thermo Triton). Instrumental mass dependent fractionation was corrected by the double-spike method as described in Heuser et al. (2002). Detailed information about the chemical procedures and mass spectrometry can be found in the Supplementary Material.

The internal precision (reproducibility) of $\delta^{44/40}$Ca values in this study is ±0.08‰ (2SE) based on 3–4 repeated measurements of each sample solution. Two standard deviations of average $\delta^{44/40}$Ca in SRM915a measured in the course of this study were ±0.13‰ ($n = 48$), which represents long-term external precision. The values for SRM915a, IAPSO Seawater, and three USGS basaltic reference samples (BCR-2, BHVO-2, and BIR-1) analyzed in the same session, as well as literature data for the same materials are reported in Table 1. The mean values of $\delta^{44/40}$Ca obtained for SRM915a and IAPSO Seawater are 0.02 ± 0.13‰ (2SD, $n = 48$) and 1.83 ± 0.13‰ (2SD, $n = 47$), respectively; those for BCR-2, BHVO-2 and BIR-1 are 0.82 ± 0.09‰ (2SD, $n = 12$), 0.80 ± 0.10‰ (2SD, $n = 16$) and 0.84 ± 0.09‰ (2SD, $n = 9$), respectively. All these results are in agreement with data in the literature (e.g. Amini et al., 2009; Feng et al., 2017; He et al., 2017; Magna et al., 2015; Huang et al., 2010; Valdes et al., 2014), which demonstrates the robustness of our analytical methods. In addition, full duplicates of 4 samples (S-14, S-62, U85 and UV-105/03) obtained by digestion of duplicate batches of rock powder show good reproducibility within the analytical errors (Table 2).

Table 1
Ca isotopic compositions of SRM915a, seawater, and USGS standards.

Samples	References	$\delta^{44/40}$Ca	2SD	*n*
SRM 915a	**This study**	**0.02**	**0.13**	**48**
	Valdes et al. (2014)	0.00	0.17	74
	Huang et al. (2010)	0.04	0.13	45
Seawater	**This study**	**1.83**	**0.12**	**47**
	Huang et al. (2010)	1.90	0.12	16
BCR-2	**This study**	**0.82**	**0.09**	**12**
	Amini et al. (2009)	0.81	0.17	6
	Valdes et al. (2014)	0.88	0.32	3
BHVO-2	**This study**	**0.80**	**0.10**	**16**
	Magna et al. (2015)	0.90	0.11	5
	Valdes et al. (2014)	0.88	0.04	13
BIR-1	**This study**	**0.84**	**0.09**	**9**
	Amini et al. (2009)	0.77	0.34	14
	Valdes et al. (2014)	0.90	0.08	4

Table 2
Ca isotopic compositions of peridotites.

Sample	Locality	Rock	CaO wt.%	Al_2O_3 wt.%	$\delta^{44/40}$Ca					Mean	2SD	2SE	n	Data source[c]
					1[a]	2	3	4	R[b]					
Group 1 fertile, unmetasomatized peridotites														
Ts-53389	Tar	Gar-Sp Lh	3.82	4.70	0.99	0.89	0.95			0.94	0.10	0.06	3	(3)
S-17	Tar	Sp Lh	3.89	4.65	0.94	0.96	0.92			0.94	0.04	0.02	3	(1)
313-8	Vit	Gar Lh	3.53	4.58	1.05	0.92	1.00			0.99	0.13	0.08	3	(4)
S-4	Tar	Sp Lh	3.92	4.48	0.93	0.98	0.93			0.95	0.06	0.03	3	(1)
313-102	Vit	Gar Lh	3.56	4.48	0.92	0.85	1.02	0.90		0.92	0.14	0.08	4	(4)
stz-1	Tar	Sp Lh	4.01	4.40	0.95	0.93	0.92			0.93	0.03	0.02	3	(2)
S-37	Tar	Sp Lh	3.25	4.39	0.91	0.94	0.94			0.93	0.03	0.02	3	(1)
S-1	Tar	Sp Lh	3.65	4.27	1.00	0.87	0.89			0.92	0.14	0.08	3	(1)
S-14	Tar	Sp Lh	3.40	4.20	0.99	0.98			0.90	0.96	0.10	0.06	3	(1)
S-21	Tar	Sp Lh	3.24	4.09	0.93	0.87	0.97			0.92	0.10	0.06	3	(1)
stz-2	Tar	Sp Lh	3.32	4.07	0.96	0.90	0.84			0.90	0.12	0.07	3	(1)
S-15	Tar	Sp Lh	3.40	4.00	0.88	0.98	0.83			0.90	0.15	0.09	3	(1)
S-2	Tar	Sp Lh	3.26	3.86	0.91	0.99	0.94			0.95	0.08	0.05	3	(1)
313-104	Vit	Gar Lh	3.49	3.66	0.98	0.90	1.03			0.97	0.13	0.08	3	(4)
Group 2 moderately refractory peridotites with LREE-depleted cpx														
S-16	Tar	Sp Lh	2.34	3.04	0.89	0.94	1.07	0.99		0.97	0.15	0.09	4	(1)
S-22	Tar	Sp Lh	1.77	2.24	0.93	0.95	1.05			0.98	0.13	0.07	3	(1)
S-62	Tar	Sp Hz	1.32	1.74	1.05	1.07			1.15	1.09	0.11	0.06	3	(1)
621-16	Vit	Gar Hz	1.07	1.31	1.18	1.02	1.05	1.03		1.07	0.15	0.09	4	(1)
BN-8	Dar	Sp Hz	0.75	1.26	1.08	1.03	0.98			1.03	0.10	0.06	3	(1)
Group 3a refractory peridotites with carbonatite-type metasomatism														
419/09	Ud	Gar Hz	1.37	1.00	0.77	0.77	0.82			0.79	0.06	0.03	3	(6)
S-29	Tar	Sp Hz	0.44	0.90	0.73	0.69	0.75			0.72	0.06	0.04	3	(1)
105/03	Ud	Sp Hz	0.33	0.67	0.54	0.70	0.53	0.61	0.66	0.61	0.15	0.09	5	(5)
H-25	Tar	Sp Hz	0.41	0.62	0.54	0.56	0.56			0.55	0.02	0.01	3	(1)
107/03	Ud	Sp Hz	0.54	0.55	0.88	1.01	0.99			0.96	0.14	0.08	3	(5)
KC-137/08	Ud	Sp Hz	0.26	0.09	0.25	0.25	0.26			0.25	0.01	0.01	3	(5)
Group 3b fertile, silicate-melt metasomatized peridotites														
4230-16	Tar	Phl Lh	3.85	4.32	0.94	0.91	0.83			0.89	0.11	0.07	3	(8)
U85	Ud	Gar Lh	3.35	3.96	0.81	0.82			0.87	0.83	0.06	0.04	3	(7)
4230-19	Tar	Phl Lh	3.11	3.92	0.92	0.90	0.82			0.88	0.11	0.06	3	(8)

The order of samples in each group is that of decreasing Al_2O_3 contents (roughly corresponds to increasing degrees of melt extraction by partial melting).
Location abbreviations: Tar, Tariat; Vi, Vitim; Dar, Dariganga; Ud, Udachnaya.
Rock type abbreviations: Lh, lherzolite; Hz, harzburgite; Gar, garnet; Sp, spinel; Phl, phlogopite.
[a] The numbers (1 to 4) represent repeated analyses of the same solution.
[b] R, full-procedure duplicate (repeated dissolution and analysis)
[c] References to data sources: (1) Unpublished data of R. Carlson and D. Ionov; (2) Press et al. (1986); (3) Ionov et al. (1998); (4) Ionov (2004); (5) Doucet et al. (2012); (6) Doucet et al. (2013); (7) Ionov et al. (2010); (8) Ionov and Hofmann (2007).

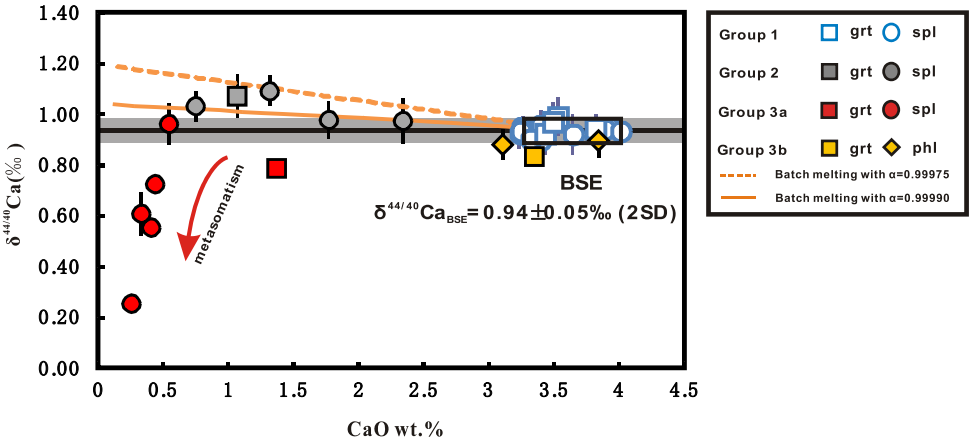

Fig. 4. A plot of $\delta^{44/40}$Ca vs. CaO. The grey field represents the BSE value estimated in this study (0.94 ± 0.05‰, 2SD). Ca isotopic variation in melting residues is calculated for pure batch melting assuming fractionation factor $\alpha_{\text{peridotite-melt}}$ ranging from 0.99975 to 0.99990. For color codes refer to the online version of the paper.

4. Results

Ca isotopic compositions are reported in Table 2 and shown in Fig. 4. The 14 Group 1 rocks (fertile, unmetasomatized spinel and garnet lherzolites) have a narrow range of $\delta^{44/40}$Ca from 0.90 ± 0.07‰ (2SE, $n = 3$) to 0.99 ± 0.08‰ (2SE, $n = 3$), with an average of 0.94 ± 0.01‰ ($n = 14$, 2SE). Two moderately melt-depleted (2.2–3.0 wt.% Al_2O_3, 1.8–2.3 wt.% CaO) Group 2 lherzolites (S-16 and S-22) have $\delta^{44/40}$Ca of 0.97 ± 0.09‰ and 0.98 ± 0.07‰ ($n \geq 3$, 2SE), close to the upper limit of the range for Group 1. By contrast, the three strongly melt-depleted (1.3–1.7 wt.% Al_2O_3, 0.8–1.3 wt.% CaO) Group 2 harzburgites from 3 localities (BN-8, 621-16 and S-62) show distinctively heavier $\delta^{44/40}$Ca values (1.03–1.09‰) with an average of 1.06 ± 0.04‰ ($n = 3$, 2SE).

The Group 3 (metasomatized) rocks have a broad $\delta^{44/40}$Ca ranging from 0.96 ± 0.08‰ ($n = 3$, 2SE) to 0.25 ± 0.01‰ ($n = 3$, 2SE), which extends to much lighter values than for samples in the other two groups (with no or only minor metasomatism). The fertile Group 3b rocks (two Phl–Sp lherzolites from Tariat and a sheared garnet lherzolite from Udachnaya) have $\delta^{44/40}$Ca from 0.83 ± 0.04‰ to 0.89 ± 0.07‰ ($n = 3$, 2SE), defining a tight cluster just below the range of unmetasomatized rocks (Fig. 4). By contrast, the $\delta^{44/40}$Ca range in the six 'anhydrous' Group 3a harzburgites from Udachnaya and Tariat (0.25–0.96‰) is much greater and includes four samples with significant low $\delta^{44/40}$Ca (0.25–0.72‰).

5. Discussion

5.1. Assessing mantle Ca isotope compositions via analyses of bulk rocks vs. minerals

The pioneering study of Huang et al. (2010) reported Ca isotope analyses of cpx and opx from two peridotite xenoliths from southwestern USA. They found that acid-leached and unleached cpx in one xenolith had similar $\delta^{44/40}$Ca, but unleached opx yielded a lower average $\delta^{44/40}$Ca than its leached fractions (1.21‰ vs. 1.40‰). Huang et al. (2010) attributed the lower $\delta^{44/40}$Ca in the unleached opx to Ca contribution from hypothetical, presumably post-eruption, low-$\delta^{44/40}$Ca carbonates precipitated on the opx surface and used only data on leached pyroxenes to constrain Ca isotope composition of "upper mantle". Yet, because no mineralogical or trace element data on the xenolith were reported by Huang et al. (2010), it is difficult to ascertain the origin of the Ca-bearing materials in the mineral separates.

It is well known, however, that mantle peridotites may contain cryptocrystalline inter-granular materials of mantle origin rich in incompatible elements (e.g. Hiraga et al., 2004). Furthermore, metasomatized mantle rocks, including Group 3 samples in this study, may contain various interstitial micro-phases, from the common amphibole and phl (e.g. Ionov et al., 1997) to more rare phosphates, carbonates, alkali feldspar, Ti-rich oxides precipitated from percolating melts and fluids (e.g. Ionov et al., 1999, 2006). For this reason, we chose to analyze bulk rock xenoliths, with the assumption that their interstitial components are mainly of mantle origin. To minimize contributions from non-mantle materials we used cores of well-studied large and fresh xenoliths with no evidence for intrusion of host basalt and no or minimal post-eruption alteration.

The first advantage of this approach is that all Ca-bearing components of bulk rocks are taken into account including those from the low-Ca olivine and potentially Ca-rich, but low-volume interstitial materials. Another one is that our Ca isotope data are direct bulk-rock measurements whereas values based on pyroxene analyses are estimates calculated using modal abundances of Ca-rich minerals, which is an indirect method to infer bulk-rock values. The latter is the case for the "upper mantle" estimates in Huang et al. (2010), which are based on approximate models for modal opx and cpx in the mantle. Finally, estimates based on cpx analyses are impossible for rocks, like harzburgite, that contain no optically recognizable cpx (e.g. two samples from this study), in cases if Ca-bearing minerals are too small for mineral picking, heterogeneous, or when their mineral proportions cannot be established reliably.

5.2. Ca isotopic composition of the BSE

The stable isotope composition of the BSE serves as a benchmark to evaluate the directions and degrees of isotope fractionation in terrestrial rocks and geochemical reservoirs. The BSE, which can be viewed as equivalent to the primitive mantle, is the silicate fraction of the Earth that remained after the separation of metallic core and loss of volatiles early in its history. It later fractionated to form the crust and the complementary melt-depleted asthenosphere and lithospheric mantle. Pioneering stable isotope studies often used data on basalts to estimate BSE values, but it is not known to what extent basaltic magmas represent the primitive mantle because: 1) partial melting may cause isotope fractionation; 2) sources of oceanic basalts vary widely; 3) magmas may fractionate and/or be contaminated by other materials upon transport and emplacement (e.g. Weyer and Ionov, 2007; Williams and Bizimis, 2014).

A more direct approach in constraining the Ca isotope composition of the BSE is to look at pristine mantle peridotites that suffered no, or only little, fractionation by melting or contamination. This approach was previously used to estimate the abundances of refractory lithophile elements including Ca in the primitive mantle, i.e. the equivalent of the BSE (McDonough and Sun, 1995). In this study, Group 1 peridotites meet these criteria, with fertile major element compositions (Fig. 2) and nearly flat or slightly LREE-depleted patterns (Fig. 3a; Ionov, 2004; Ionov and Hofmann, 2007; Press et al., 1986), and thus are appropriate to estimate Ca isotope composition of the BSE. Notably, our Vitim samples were previously used to constrain Li, Mg, V, and Zn isotopic compositions of the BSE and yielded uniform isotope values within a given isotope system (Doucet et al., 2016; Pogge von Strandmann et al., 2011; Prytulak et al., 2013). Here, we estimate the $\delta^{44/40}$Ca of BSE to be 0.94 ± 0.05‰ (2SD) as a mean of average (3–4 duplicates) analyses of the 14 Group 1 lherzolites. Importantly, $\delta^{44/40}$Ca in the four garnet and garnet-spinel lherzolites match those of spinel lherzolites, showing no differences between the spinel and garnet facies mantle (Fig. 4).

Magna et al. (2015) suggested that because the Ca–O bonds in garnet are shorter than in cpx, and because heavy isotopes prefer stronger bonding environments, garnets may have higher $\delta^{44/40}$Ca than the coexisting cpx. This argument, however, if valid, only concerns inter-mineral isotope fractionation, but does not imply that garnet peridotites in general have heavier Ca isotopes than garnet-free peridotites because there is no net mass transfer during the transformation of spinel to garnet peridotites thus precluding Ca isotope fractionation.

5.3. Ca isotope fractionation during mantle melting

Calcium is preferentially partitioned into melt and is depleted in residues during melting of peridotite. Cpx, the most important silicate host of Ca in the fertile upper mantle, with ~20% CaO, is exhausted at ≥25% melting at 0–2 GPa (e.g., Pickering-Witter and Johnston, 2000). The effects of melt extraction on the Ca isotopic composition of melting residues are examined here by comparing the Group 1 fertile rocks with the Group 2 melt-depleted, unmetasomatized peridotites.

While the two moderately melt-depleted (2.2–3.0 wt.% Al_2O_3, 1.8–2.3 wt.% CaO) Group 2 lherzolites show $\delta^{44/40}$Ca values (0.97 ± 0.09‰ to 0.98 ± 0.07‰) near the upper limit of the Group 1 range, the three strongly melt-depleted (0.75–1.3 wt.% Al_2O_3, 0.8–1.7 wt.% CaO) Group 2 harzburgites have considerably higher $\delta^{44/40}$Ca, 1.03 ± 0.06 to 1.09 ± 0.06‰. These harzburgites are residues of much greater melt-extraction degrees than the lherzolites, i.e. ~25–30% vs. <20% of isobaric batch melting at 4 GPa (Fig. 2). Furthermore, because the LREE-depleted cpx patterns in the Group 2 harzburgites (Fig. 3b) indicate little (if any) metasomatic influence (Ionov et al., 2005; Press et al., 1986), the higher $\delta^{44/40}$Ca most likely reflect the effects of mantle partial melting. Given that the fractionation scale of Ca isotopes during partial melting is relatively small, partial melting-induced Ca isotopic shift can only be distinguished in highly melt-depleted peridotites (25–30% melting, Fig. 2b) with the analytical uncertainty in this study (~0.13‰).

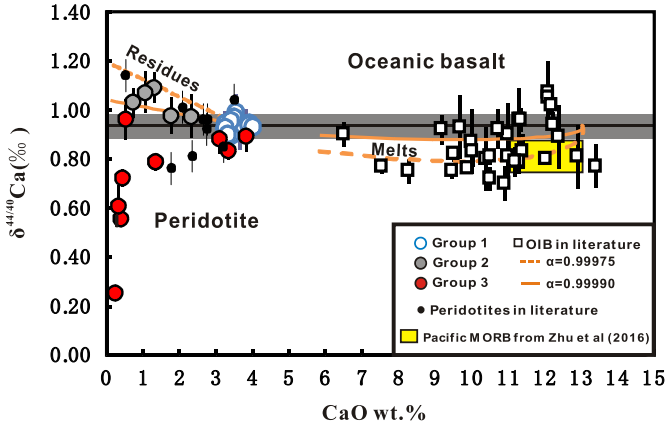

Fig. 5. Comparison of mantle peridotites with oceanic basalts (OIB and MORB) on a plot of $\delta^{44/40}$Ca vs. CaO. Grey field represents the BSE value from this study. Modeling results for residues and partial melts of pure batch melting of the BSE are shown assuming $\alpha_{\text{peridotite-melt}}$ ranging from 0.99975 to 0.99990. Literature data of peridotites are from Amini et al. (2009) and Kang et al. (2016). OIB data are from Amini et al. (2009), Huang et al. (2011), Valdes et al. (2014) and Jacobson et al. (2015). The range of $\delta^{44/40}$Ca for the Pacific MORB is from Zhu et al. (2016). Some oceanic basalt data plotted in Fig. 1 are not included in this figure because their CaO contents are not published.

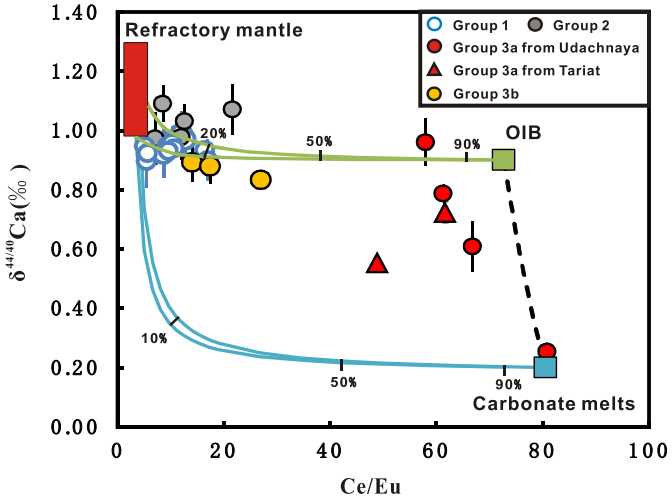

Fig. 6. A plot of $\delta^{44/40}$Ca vs. Ce/Eu for peridotites in this study. Simple binary mixing between carbonate melts and refractory mantle (blue curve) cannot explain the variations of Ca isotopes and Ce/Eu in Udachnaya harzburgites. A mixing model for three end-members, carbonate melt, OIB-like silicate melt and refractory mantle, is applied to examine the $\delta^{44/40}$Ca and Ce/Eu variations. The percentages besides the curve denote the contribution of metasomatism agents to the REE budget. The parameters and references for the model are given in supplementary material. For color codes refer to the online version of the paper.

Earlier studies have suggested that cpx (CaO ~20.0 wt.%) may have lighter Ca isotopic composition than coexisting olivine (CaO <0.1 wt.%), opx (CaO <1.5 wt.%), and garnet (CaO ~3–5 wt.%) (Feng et al., 2014; Huang et al., 2010; Kang et al., 2016; Magna et al., 2015). Because modal abundances of cpx decrease whereas those of olivine and opx increase in residues at higher melting degrees, the residues may be progressively enriched in heavy Ca isotopes with the exhaustion of cpx, which is generally consistent with our data for the Group 2 and Group 1 rocks.

To provide quantitative constraints on the fractionation factor between peridotite and melt ($\alpha_{\text{peridotite-melt}}$), modal batch melting modeling similar to that in Weyer and Ionov (2007) and Doucet et al. (2016) was applied. In this model, CaO variations in residues and partial melts were estimated with the method of Niu (1997) initially applied to abyssal peridotites. Details of the modeling are given in Supplementary Material. As shown in Figs. 4 and 5, the modeling suggests that the variations of $\delta^{44/40}$Ca in the melt-depleted peridotites can be explained by melting of fertile mantle at 3 GPa with $\alpha_{\text{peridotite-melt}}$ ranging from 0.99975 to 0.99990 ($10^3 \ln\alpha_{\text{peridotite-melt}} \approx 0.10$–$0.25$). However, this estimate is approximate because the fractionation factor may vary with cpx consumption and also depend on P–T conditions, like for Zn isotopes (Doucet et al., 2016).

5.4. Ca isotopic composition of metasomatized peridotites

The notion of mantle metasomatism includes a broad range of phenomena taking place in melt-depleted residues due to reaction with migrating melts or fluids. Initially, such residues are depleted in incompatible elements and may contain no or only small amounts of Ca-rich minerals (cpx, garnet), but interaction with metasomatic media may cause important changes in their chemical (cryptic), and possibly modal compositions (patent or modal) (e.g. Bodinier et al., 1990). Cryptic metasomatism produces enrichments in incompatible elements, notably in LREE over MREE-HREE (Fig. 3c–d) without apparent changes in phase assemblage. Modal metasomatism, in addition, precipitates new phases, like water-bearing amphibole and phl (e.g. Ionov et al., 1997) as well as Ca-rich cpx, carbonates, phosphates, and alkali feldspar (e.g. Ionov et al., 1999, 2006).

In general, the peridotites affected by mantle metasomatism in this study tend to have lower $\delta^{44/40}$Ca values than fertile (0.90–0.97‰) or melt-depleted (0.97–1.09‰) rocks, which we attribute to reaction of the latter with lighter, Ca-rich fluids/melts. In detail, out of nine metasomatized samples in this study, the three Group 3b fertile lherzolites show a tight $\delta^{44/40}$Ca range from 0.83‰ to 0.89‰, which is only slightly lighter than the BSE. By contrast, the six Group 3a harzburgites display a much broader $\delta^{44/40}$Ca range from 0.25‰ to 0.96‰. The $\delta^{44/40}$Ca in the metasomatized rocks may be controlled by (a) the nature of metasomatic media, (b) degree and type of metasomatism, (c) the composition of the rocks that undergo metasomatism, and (d) diffusion-related isotope fractionation during melt percolation. These factors are examined below for subgroups 3a and 3b.

5.4.1. Very light Ca isotope compositions in Group 3a

Highly refractory, olivine-rich rocks, like the Group 3a harzburgites in this study, are most likely to be intruded and metasomatized by migrating melts (e.g. Frey and Green, 1974) because they are most permeable for porous melt flow (e.g. Toramaru and Fujii, 1986), in particular for carbonate-rich melts (Hunter and McKenzie, 1989). Furthermore, because such refractory residues are low in Ca, metasomatic additions of Ca or equilibration with percolating melts may modify their Ca isotopic compositions much more than those of Ca-rich fertile peridotites. As a result, the Ca isotope compositions of such strongly metasomatized, refractory peridotites may mainly reflect the nature of the metasomatic media.

The six Group 3a harzburgites (four from Udachnaya and two from Tariat) show a positive correlation of $\delta^{44/40}$Ca with CaO (Fig. 4) and negative correlations with LREE/MREE ratios (e.g. Ce/Eu, Fig. 6), which we view as evidence for links of their Ca isotopic composition with metasomatism. Notably, the most refractory Udachnaya peridotite in this study, cpx-free KC-137/08, has the lightest $\delta^{44/40}$Ca of 0.25‰ and a very high Ce/Eu of 81, the latter identical to Ce/Eu for an average of fresh Udachnaya kimberlites (Kamenetsky et al., 2012).

Primary kimberlite magmas are CO_2-rich and appear to be generated from rocks enriched in carbonates and incompatible elements by sub-lithospheric fluids (e.g. le Roex et al., 2003). Kamenetsky et al. (2012) argued that the parental melt of the Udachnaya kimberlite (and possibly of Type I kimberlites worldwide) was a halogen-rich Na–Ca carbonatite, which progressively

assimilated silicate components to form kimberlite magmas. All these melts intruded host mantle and metasomatized it. The Udachnaya samples in this study contain no kimberlite veins and related phl–cpx pockets, hence their budgets of incompatible components are related to metasomatism in the mantle and not to ingress of kimberlite to xenoliths during their transport (Agashev et al., 2013; Doucet et al., 2013). Carbonate-rich media were also inferred as likely metasomatic agents for Tariat harzburgites, which often contain microcrystalline apatite (Ionov, 2007; Ionov et al., 2006).

It was recently suggested, based on studies of mantle-derived rocks from eastern China affected by Meso-Cenozoic subduction, that subduction-related melts or fluids could impart low-$\delta^{44/40}$Ca signatures to peridotites because some recycled marine carbonates have lower $\delta^{44/40}$Ca (-1.09 to 1.81‰ with an average of 0.61‰, Fantle and Tipper, 2014) than the upper mantle (Kang et al., 2016). There is no evidence however that the mantle beneath Udachnaya ($\geq$1000 km from the margins of the Siberian craton), or beneath central Mongolia, could be directly affected by subduction-derived fluids either at the time of the eruption or earlier in its history. Alternatively, recycled carbonates with light Ca-isotope signatures could be first subducted to the deep mantle and to be later brought up by mantle upwelling to source regions of intra-plate magmas (Ionov et al., 2006; Moyen et al., 2017).

As shown in Fig. 6, the correlation between $\delta^{44/40}$Ca and Ce/Eu in the Group 3a samples cannot be explained by binary mixing of refractory peridotites and a single carbonate melt end-member (find the modeling parameters in S-Table 2 of Supplementary material). This feature, however, is consistent with the complex evolution of Udachnaya kimberlite magmas, which is related to reactions of the parental alkali-CO_2-halogen-rich fluids with the host mantle to gradually increase its silicate contents. Hence, both carbonatite melts and related metasomatic media could have a large range of $\delta^{44/40}$Ca and Ce/Eu. Likewise, Ionov et al. (2010) and Agashev et al. (2013) argued that Udachnaya peridotites experienced multiple stages of enrichments, first by carbonatite then by OIB-like silicate liquids. It is thus possible that the relationship between Ce/Eu and $\delta^{44/40}$Ca in the Group 3a rocks reflects a net result of multiple metasomatic events by evolving CO_2-rich media, shown as the three-end-member mixing model in Fig. 6.

An additional mechanism to yield light Ca isotopic values in metasomatized rocks could be kinetic isotope fractionation previously proposed for stable isotopes of other elements in mantle peridotites, e.g. Fe (Weyer and Ionov, 2007) and Li (Rudnick and Ionov, 2007). Because lighter isotopes diffuse faster they may be locally enriched at a metasomatic front or in melt-rock reactions. Such 'chromatographic' effects were earlier invoked to explain the decoupling of trace elements (e.g. Bodinier et al., 1990; Ionov et al., 2002a) and Sr and Nd isotopes (Ionov et al., 2002b) in enriched peridotites.

5.4.2. Moderately-light Ca isotopic composition of Group 3b samples

The metasomatic effects on Ca isotopes in the three patently metasomatized Group 3b lherzolites (two phl-bearing spinel lherzolites from Tariat and a sheared garnet lherzolite from Udachnaya) are uniformly minor, with only slightly lighter $\delta^{44/40}$Ca (0.83–0.89‰) than the BSE value, in spite of evidence for equilibration with metasomatic media like LREE-enriched, concave down REE patterns (Fig. 3d) and texturally equilibrated phl in the Tariat xenoliths (Ionov et al., 2002a; Ionov and Hofmann, 1995). This difference may be due either to low mass ratios of Ca in the metasomatic media to Ca in the host peridotites with high CaO (3.1–3.9 wt.% in Group 3b rocks) or alternatively, much smaller differences between Ca isotopic composition of the pre-metasomatic rocks and the metasomatic media.

5.5. Relationships between $\delta^{44/40}$Ca of the mantle and oceanic basalts

A compilation of published Ca isotope data on basalts (Fig. 1) shows a large range from 0.62 to 1.54‰ with an average of 0.90 $\pm$ 0.28‰ ($n = 61$, 2SD) (data from Amini et al., 2009; Huang et al., 2010, 2011; Holmden and Bélanger, 2010; Hindshaw et al., 2013; Jacobson et al., 2015; Skulan et al., 1997; Simon and DePaolo, 2010; Valdes et al., 2014). A recent study by Zhu et al. (2016) shows that $\delta^{44/40}$Ca in normal and depleted MORB from the Pacific Ocean range from 0.75 to 0.88‰ with an average of 0.83 ± 0.07‰ (2SE, $n = 13$). Such variations can be explained by equilibrium Ca-isotope fractionation during mantle melting (Fig. 5). Much more fractionated $\delta^{44/40}$Ca in oceanic basalts (0.62–1.54‰, 60 samples, Figs. 1 and 5) can be due to several factors. Interaction with seawater, which has a high $\delta^{44/40}$Ca value of $\sim$1.82‰ (e.g. Fantle and Tipper, 2014 and references therein), may elevate their $\delta^{44/40}$Ca values (e.g., John et al., 2012). Further, crustal materials like sediments and carbonates may have much lighter Ca isotopic composition than the BSE (Fantle and Tipper, 2014 and references therein). Incorporation of such isotopically lighter materials in the source regions of basaltic magmas may lower their $\delta^{44/40}$Ca values, in which case Ca isotopes in basalts could serve as recycling tracers (e.g. Huang et al., 2011). On the other hand, the effects of partial melting should also be taken into account. Our modeling suggests that melts derived from pristine mantle may have $\delta^{44/40}$Ca from 0.79 to 0.94‰ depending on melting degrees and fractionation factors (Fig. 5). Thus, we suggest that $\delta^{44/40}$Ca < 0.79‰ in basalts may be seen as indication of the contribution of recycled isotopically lighter materials in their mantle sources.

5.6. Interplanetary comparisons

Our new estimate of the $\delta^{44/40}$Ca in the BSE may help evaluate likely building blocks of the Earth. As shown in Fig. 7, achondrites and ordinary chondrites have $\delta^{44/40}$Ca ranging from 0.88 to 1.13‰ (e.g., Huang and Jacobsen, 2017; Simon and DePaolo, 2010; Valdes et al., 2014), i.e. close to the BSE estimate (0.94 ± 0.05‰) obtained in this study. The Ca isotopic composition of the majority of Martian meteorites is similar to our BSE estimate as well (Magna et al., 2015; Simon and DePaolo, 2010). By comparison, carbonaceous chondrites display a broad $\delta^{44/40}$Ca range of 0.27–1.19‰ (Huang and Jacobsen, 2017; Simon and DePaolo, 2010; Valdes et al., 2014; Amsellem et al., 2017), with CM, CV3, CR2 and CI isotopically lighter than the BSE and most CO similar to the BSE. Such variations may be caused by disequilibrium condensation of the solar nebula or be related to the Calcium–Aluminium-rich Inclusions, CAI's (Simon and DePaolo, 2010). In contrast, some enstatite chondrites have heavier Ca isotopic compositions (0.90–1.51‰) than the BSE, casting doubts on their role as possible Earth's building blocks. Valdes et al. (2014) attributed this signature to variations in modal proportions of oldhamite, which is enriched in heavy Ca isotopes relative to silicate phases of enstatite chondrites. More work is needed to understand the implications of Ca isotope compositions of the rocky planets and meteorites.

The Earth–Moon system has been proposed to form by collision of the proto-Earth with a Mars-sized impactor named Theia (e.g. Cameron, 2001). The Ca isotopic compositions of several lunar samples reported by Simon and DePaolo (2010) and Valdes et al. (2014) are consistent with the BSE estimate in this study (Fig. 6). Such a consistent Ca isotopic signature is reminiscent of the identical O and Ti isotopic compositions of terrestrial and lunar samples (e.g., Wiechert et al., 2001), which supports the hypothesis that the majority of the Moon-forming materials came from the proto-Earth rather than Theia (e.g. Zhang et al., 2012).

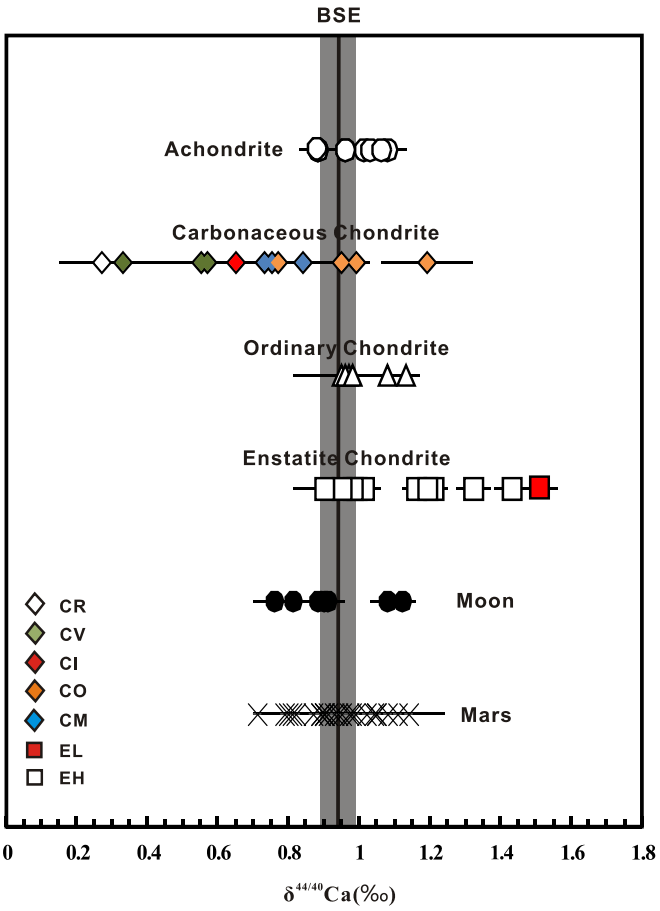

Fig. 7. A compilation of Ca isotopic data for primitive meteorites, lunar samples, and Martian meteorites. The gray vertical band represents the $\delta^{44/40}$Ca of the BSE, i.e. 0.94 ± 0.05‰ (2SD, $n = 14$) estimated in this study. Data sources: primitive meteorite data, Simon and DePaolo (2010) and Valdes et al. (2014), lunar samples, Valdes et al. (2014), and Martian meteorites, Simon and DePaolo (2010) and Magna et al. (2015). Achondrite data include those for aubrite, angrite, diogenite, and eucrite. Carbonaceous chondrite data include those for the CM, CV, CO, CR and CI types. Ordinary chondrite data include those for LL and L. Enstatite chondrite data include those for the EH and EL types.

6. Summary and conclusions

We report whole-rock Ca isotope data for three groups of well-studied peridotite xenoliths from central Asia and the Siberian craton to constrain Ca isotopic composition of the BSE and explore Ca isotope fractionation in the upper mantle.

(1) Fertile spinel and garnet lherzolites (Group 1) show identical $\delta^{44/40}$Ca, their average defines a $\delta^{44/40}$Ca for BSE of 0.94 ± 0.05‰ (2SD, $n = 14$).

(2) The average $\delta^{44/40}$Ca (1.07 ± 0.04‰, $n = 3$) of harzburgites without significant metasomatism (Group 2) is slightly higher than the BSE value, suggesting that partial melting may induce observable Ca isotopic fractionation in refractory peridotites and in complementary melts at melting degrees ≥20%. A modal batch-melting model with $\alpha_{\text{peridotite-melt}}$ ranging from 0.99975 to 0.99990 can explain our data.

(3) Ca isotope variations in metasomatized peridotites are largely controlled by the nature of metasomatic media, degree and type of metasomatism, and the Ca contents of the initial rocks. Metasomatized, low-Ca harzburgites (Group 3a) have a broad range of $\delta^{44/40}$Ca from 0.25 ± 0.01‰ to 0.96‰ $\pm$ 0.08‰ that are negatively correlated with LREE/MREE ratios. Their light Ca isotope compositions may be imparted by a range of metasomatic media from carbonatites to proto-kimberlitic liquids, possibly containing recycled crustal components. $\delta^{44/40}$Ca in metasomatized fertile peridotites (Group 3b) are only slightly lighter (0.83–0.89‰) than in the BSE, possibly due to low mass ratios of Ca in the metasomatic media to Ca in the host peridotites or smaller Ca isotope differences between these two components.

Acknowledgements

This work was supported by the Strategic Priority Research Program (B) of the Chinese Academy of Sciences (XDB18000000), the National Science Foundation of China (41325011, 41573017) and the 111 project. DAI acknowledges funding from the French CNRS (INSU-PNP annual grants in 2010–17 for mantle studies), AVG was supported by Russian State Assignment Project No. 0330-2016-0006. We thank Hongli Zhu with discussion and the help of analysis, Maria C. Valdes for data on some basalts, Gui-Qin Wang for help with isotope analyses and Chen Zhu and Anne Hereford for help with polishing English.

Appendix A. Supplementary material

Supplementary material related to this article can be found online at http://dx.doi.org/10.1016/j.epsl.2017.05.035.

References

Agashev, A.M., Ionov, D.A., Pokhilenko, N.P., Golovin, A.V., Cherepanova, Y., Sharygin, I.S., 2013. Metasomatism in lithospheric mantle roots: constraints from whole-rock and mineral chemical composition of deformed peridotite xenoliths from kimberlite pipe Udachnaya. Lithos 160–161, 201–215.

Amini, M., Eisenhauer, A., Böhm, F., Holmden, C., Kreissig, K., Hauff, F., Jochum, K.P., 2009. Calcium Isotopes ($\delta^{44/40}$Ca) in MPI-DING reference glasses, USGS rock powders and various rocks: evidence for ca isotope fractionation in terrestrial silicates. Geostand. Geoanal. Res. 33, 231–247.

Amsellem, E., Moynier, F., Pringle, E.A., Bouvier, A., Chen, H., Day, J.M., 2017. Testing the chondrule-rich accretion model for planetary embryos using calcium isotopes. Earth Planet. Sci. Lett. 469, 75–83.

Bodinier, J.-L., Vasseur, G., Vernières, J., Dupuy, C., Fabriès, J., 1990. Mechanisms of mantle metasomatism: geochemical evidence from the Lherz orogenic peridotite. J. Petrol. 31, 597–628.

Cameron, A.G.W., 2001. From interstellar gas to the Earth–Moon system. Meteorit. Planet. Sci. 36, 9–22.

Chen, H., Savage, P.S., Teng, F.Z., Helz, R.T., Moynier, F., 2013. Zinc isotope fractionation during magmatic differentiation and the isotopic composition of the bulk Earth. Earth Planet. Sci. Lett. 369–370, 34–42.

DePaolo, D.J., 2004. Calcium isotopic variations produced by biological, kinetic, radiogenic and nucleosynthetic processes. Rev. Mineral. Geochem. 55, 255–288.

Doucet, L.S., Ionov, D.A., Golovin, A.V., Pokhilenko, N.P., 2012. Depth, degrees and tectonic settings of mantle melting during craton formation: inferences from major and trace element compositions of spinel harzburgite xenoliths from the Udachnaya kimberlite, central Siberia. Earth Planet. Sci. Lett. 359–360, 206–218.

Doucet, L.S., Ionov, D.A., Golovin, A.V., 2013. The origin of coarse garnet peridotites in cratonic lithosphere: new data on xenoliths from the Udachnaya kimberlite, central Siberia. Contrib. Mineral. Petrol. 165, 1225–1242.

Doucet, L.S., Mattielli, N., Ionov, D.A., Debouge, W., Golovin, A.V., 2016. Zn isotopic heterogeneity in the mantle: A melting control? Earth Planet. Sci. Lett. 451, 232–240.

Fantle, M.S., Tipper, E.T., 2014. Calcium isotopes in the global biogeochemical Ca cycle: implications for development of a Ca isotope proxy. Earth-Sci. Rev. 129, 148–177.

Feng, C., Qin, T., Huang, S., Wu, Z., Huang, F., 2014. First-principles investigations of equilibrium calcium isotope fractionation between clinopyroxene and Ca-doped orthopyroxene. Geochim. Cosmochim. Acta 143, 132–142.

Feng, L.P., Zhou, L., Yang, L., DePaolo, D.J., Tong, S.Y., Liu, Y.S., Gao, S., 2017. Calcium isotopic compositions of sixteen USGS reference materials. Geostand. Geoanal. Res. 41, 93–106. http://dx.doi.org/10.1111/ggr.12131.

Frey, F.A., Green, D.H., 1974. The mineralogy, geochemistry and origin of lherzolite inclusions in Victorian basanites. Geochim. Cosmochim. Acta 38, 1023–1059.

He, Y., Wang, Y., Zhu, C., Huang, S., Li, S., 2017. Mass independent and mass dependent Ca isotopic compositions of thirteen geological reference materials measured by thermal ionisation mass spectrometry. Geostand. Geoanal. Res. 41, 283–302.

Herzberg, C., 2004. Geodynamic information in peridotite petrology. J. Petrol. 45, 2507–2530.

Heuser, A., Eisenhauer, A., Gussone, N., Bock, B., Hansen, B.T., Nägler, T.F., 2002. Measurement of calcium isotopes (δ^{44}Ca) using a multi-collector TIMS technique. Int. J. Mass Spectrom. 220 (3), 385–397.
Hindshaw, R.S., Bourdon, B., Pogge von Strandmann, P.A., Vigier, N., Burton, K.W., 2013. The stable calcium isotopic composition of rivers draining basaltic catchments in Iceland. Earth Planet. Sci. Lett. 374, 173–184.
Hiraga, T., Anderson, I.M., Kohlstedt, D.L., 2004. Grain boundaries as reservoirs of incompatible elements in the Earth's mantle. Nature 427, 699–703.
Hofmann, A.W., 2014. Sampling Mantle Heterogeneity through Oceanic Basalts: Isotopes and Trace Elements, 2nd edition. Treatise on Geochemistry, vol. 3. Elsevier, Oxford, pp. 67–101.
Holmden, C., Bélanger, N., 2010. Ca isotope cycling in a forested ecosystem. Geochim. Cosmochim. Acta 74, 995–1015.
Huang, S., Jacobsen, S.B., 2017. Calcium isotopic compositions of chondrites. Geochim. Cosmochim. Acta 201, 364–376.
Huang, S., Farkaš, J., Jacobsen, S.B., 2010. Calcium isotopic fractionation between clinopyroxene and orthopyroxene from mantle peridotites. Earth Planet. Sci. Lett. 292, 337–344.
Huang, S., Farkaš, J., Jacobsen, S.B., 2011. Stable calcium isotopic compositions of Hawaiian shield lavas: evidence for recycling of ancient marine carbonates into the mantle. Geochim. Cosmochim. Acta 75, 4987–4997.
Huang, S., Farkaš, J., Yu, G., Petaev, M.I., Jacobsen, S.B., 2012. Calcium isotopic ratios and rare earth element abundances in refractory inclusions from the Allende CV3 chondrite. Geochim. Cosmochim. Acta 77, 252–265.
Hunter, R.H., McKenzie, D., 1989. The equilibrium geometry of carbonate melts in rocks of mantle composition. Earth Planet. Sci. Lett. 92, 347–356.
Ionov, D.A., 2004. Chemical variations in peridotite xenoliths from Vitim, Siberia: inferences for REE and Hf behaviour in the garnet facies upper mantle. J. Petrol. 45, 343–367.
Ionov, D.A., 2007. Compositional variations and heterogeneity in fertile lithospheric mantle: peridotite xenoliths in basalts from Tariat, Mongolia. Contrib. Mineral. Petrol. 154, 455–477.
Ionov, D.A., Hofmann, A.W., 1995. Nb–Ta-rich mantle amphiboles and micas: implications for subduction-related metasomatic trace element fractionations. Earth Planet. Sci. Lett. 131, 341–356.
Ionov, D.A., Hofmann, A.W., 2007. Depth of formation of sub-continental off-craton peridotites. Earth Planet. Sci. Lett. 261, 620–634.
Ionov, D.A., Hoefs, J., Wedepohl, K.H., Wiechert, U., 1992. Content and isotopic composition of sulphur in ultramafic xenoliths from central Asia. Earth Planet. Sci. Lett. 111, 269–286.
Ionov, D.A., Ashchepkov, I.V., Stosch, H.G., Witt-Eickschen, G., Seck, H.A., 1993. Garnet peridotite xenoliths from the Vitim volcanic field, Baikal region: the nature of the garnet-spinel peridotite transition zone in the continental mantle. J. Petrol. 34, 1141–1175.
Ionov, D.A., O'Reilly, S.Y., Griffin, W.L., 1997. Volatile-bearing minerals and lithophile trace elements in the upper mantle. Chem. Geol. 141, 153–184.
Ionov, D.A., O'Reilly, S.Y., Griffin, W.L., 1998. A geotherm and lithospheric cross-section for central Mongolia. In: Flower, M.J.F., Chung, S.-L., Lo, C.-H., Lee, T.Y. (Eds.), Mantle Dynamics and Plate Interactions in East Asia. In: Geodynamics Ser., vol. 27. Amer. Geophys. Union, Washington, DC, pp. 127–153.
Ionov, D.A., Grégoire, M., Prikhod'ko, V.S., 1999. Feldspar-Ti-oxide metasomatism in off-cratonic continental and oceanic upper mantle. Earth Planet. Sci. Lett. 165, 37–44.
Ionov, D.A., Bodinier, J.-L., Mukasa, S.B., Zanetti, A., 2002a. Mechanisms and sources of mantle metasomatism: major and trace element compositions of peridotite xenoliths from Spitsbergen in the context of numerical modeling. J. Petrol. 43, 2219–2259.
Ionov, D.A., Mukasa, S.B., Bodinier, J.-L., 2002b. Sr–Nd–Pb isotopic compositions of peridotite xenoliths from Spitsbergen: numerical modelling indicates Sr–Nd decoupling in the mantle by melt percolation metasomatism. J. Petrol. 43, 2261–2278.
Ionov, D.A., Ashchepkov, I., Jagoutz, E., 2005. The provenance of fertile off-craton lithospheric mantle: Sr–Nd isotope and chemical composition of garnet and spinel peridotite xenoliths from Vitim, Siberia. Chem. Geol. 217, 41–75.
Ionov, D.A., Hofmann, A.W., Merlet, C., Gurenko, A.A., Hellebrand, E., Montagnac, G., Gillet, P., Prikhodko, V.S., 2006. Discovery of whitlockite in mantle xenoliths: inferences for water- and halogen-poor fluids and trace element residence in the terrestrial upper mantle. Earth Planet. Sci. Lett. 244, 201–217.
Ionov, D.A., Doucet, L.S., Ashchepkov, I.V., 2010. Composition of the lithospheric mantle in the Siberian craton: new constraints from fresh peridotites in the Udachnaya-East kimberlite. J. Petrol. 51, 2177–2210.
Jacobson, A.D., Andrews, M.G., Lehn, G.O., Holmden, C., 2015. Silicate versus carbonate weathering in Iceland: new insights from Ca isotopes. Earth Planet. Sci. Lett. 416, 132–142.
John, T., Gussone, N., Podladchikov, Y.Y., Bebout, G.E., Dohmen, R., Halama, R., Klemd, R., Magna, T., Seitz, H.M., 2012. Volcanic arcs fed by rapid pulsed fluid flow through subducting slabs. Nat. Geosci. 5, 489–492.
Kamenetsky, V.S., Kamenetsky, M.B., Golovin, A.V., Sharygin, V.V., Maas, R., 2012. Ultrafresh salty kimberlite of the Udachnaya–East pipe (Yakutia, Russia): a petrological oddity or fortuitous discovery? Lithos 152, 173–186.
Kang, J.-T., Zhu, H.-L., Liu, Y.-F., Liu, F., Wu, F., Hao, Y.-T., Zhi, X.-C., Zhang, Z.-F., Huang, F., 2016. Calcium isotopic composition of mantle xenoliths and minerals from Eastern China. Geochim. Cosmochim. Acta 174, 335–344.
le Roex, A.P., Bell, D.R., Davis, P., 2003. Petrogenesis of group I kimberlites from Kimberley, South Africa: evidence from bulk-rock geochemistry. J. Petrol. 44, 2261–2286.
Lodders, K., 2003. Solar system abundances and condensation temperatures of the elements. Astrophys. J. 591, 1220–1247.
Magna, T., Gussone, N., Mezger, K., 2015. The calcium isotope systematics of Mars. Earth Planet. Sci. Lett. 430, 86–94.
McDonough, W.F., Sun, S.-S., 1995. The composition of the Earth. Chem. Geol. 120, 223–253.
Moyen, J.-F., Paquette, J.L., Ionov, D.A., Gannoun, A., Korsakov, A.V., Golovin, A.V., Moine, B.N., 2017. Paleoproterozoic rejuvenation and replacement of Archaean lithosphere: evidence from zircon U–Pb dating and Hf isotopes in crustal xenoliths at Udachnaya, Siberian craton. Earth Planet. Sci. Lett. 457, 149–159.
Niu, Y., 1997. Mantle melting and melt extraction processes beneath ocean ridges: evidence from abyssal peridotites. J. Petrol. 38, 1047–1074.
Pickering-Witter, J., Johnston, A.D., 2000. The effects of variable bulk composition on the melting systematics of fertile peridotitic assemblages. Contrib. Mineral. Petrol. 140, 190–211.
Pogge von Strandmann, P.A.E., Elliott, T., Marschall, H.R., Coath, C., Lai, Y.J., Jeffcoate, A.B., Ionov, D.A., 2011. Variations of Li and Mg isotope ratios in bulk chondrites and mantle xenoliths. Geochim. Cosmochim. Acta 75, 5247–5268.
Press, S., Witt, G., Seck, H.A., Eonov, D., Kovalenko, V.I., 1986. Spinel peridotite xenoliths from the Tariat Depression, Mongolia. I: Major element chemistry and mineralogy of a primitive mantle xenolith suite. Geochim. Cosmochim. Acta 50, 2587–2599.
Prytulak, J., Nielsen, S.G., Ionov, D.A., Halliday, A.N., Harvey, J., Kelley, K.A., Niu, Y.L., Peate, D.W., Shimizu, K., Sims, K.W.W., 2013. The stable vanadium isotope composition of the mantle and mafic lavas. Earth Planet. Sci. Lett. 365, 177–189.
Rudnick, R.L., Gao, S., 2003. Composition of the continental crust. In: Treatise on Geochemistry, vol. 3. Elsevier, Oxford, pp. 1–64.
Rudnick, R.L., Ionov, D.A., 2007. Lithium elemental and isotopic disequilibrium in minerals from peridotite xenoliths from far-east Russia: product of recent melt/fluid-rock reaction. Earth Planet. Sci. Lett. 256 (1–2), 278–293.
Schiller, M., Gussone, N., Wombacher, F., 2016. High temperature geochemistry and cosmochemistry. In: Calcium Stable Isotope Geochemistry. Springer, Berlin, Heidelberg, pp. 223–245.
Simon, J.I., DePaolo, D.J., 2010. Stable calcium isotopic composition of meteorites and rocky planets. Earth Planet. Sci. Lett. 289, 457–466.
Skulan, J., DePaolo, D.J., Owens, T.L., 1997. Biological control of calcium isotopic abundances in the global calcium cycle. Geochim. Cosmochim. Acta 61, 2505–2510.
Teng, F.-Z., Wadhwa, M., Helz, R.T., 2007. Investigation of magnesium isotope fractionation during basalt differentiation: implications for a chondritic composition of the terrestrial mantle. Earth Planet. Sci. Lett. 261, 84–92.
Toramaru, A., Fujii, N., 1986. Connectivity of melt phase in a partially molten peridotite. J. Geophys. Res. 91, 9239–9252.
Valdes, M.C., Moreira, M., Foriel, J., Moynier, F., 2014. The nature of Earth's building blocks as revealed by calcium isotopes. Earth Planet. Sci. Lett. 394, 135–145.
Weyer, S., Ionov, D.A., 2007. Partial melting and melt percolation in the mantle: the message from Fe isotopes. Earth Planet. Sci. Lett. 259, 119–133.
Wiechert, U., Ionov, D.A., Wedepohl, K.H., 1997. Spinel peridotite xenoliths from the Atsagin-Dush volcano, Dariganga lava plateau, Mongolia: a record of partial melting and cryptic metasomatism in the upper mantle. Contrib. Mineral. Petrol. 126, 345–364.
Wiechert, U., Halliday, A.N., Lee, D.C., Snyder, G.A., Taylor, L.A., Rumble, D., 2001. Oxygen isotopes and the Moon-forming giant impact. Science 294, 345–348.
Williams, H.M., Bizimis, M., 2014. Iron isotope tracing of mantle heterogeneity within the source regions of oceanic basalts. Earth Planet. Sci. Lett. 404, 396–407.
Zhang, J., Dauphas, N., Davis, A.M., Leya, I., Fedkin, A., 2012. The proto-Earth as a significant source of lunar material. Nature Geosci. 5 (4), 251–255.
Zhu, H.L., Zhang, Z.F., Sun, W.D., 2016. Calcium isotopic fractionation during partial melting: constraints from mid-ocean ridge basalts. Goldschmidt Conf. Abstr. 2016, 1365.